



Adaptive location method for film cooling holes based on the design intent of the turbine blade

Yaohua Hou¹ · Jing Wang¹ · Jiawei Mei² · Hualong Zhao¹

Received: 2 August 2023 / Accepted: 13 March 2024 / Published online: 21 March 2024
© The Author(s), under exclusive licence to Springer-Verlag London Ltd., part of Springer Nature 2024

Abstract

Due to the inevitable deviation of the casting process, the dimensional error of the turbine blade is introduced. As a result, the location datum of the film cooling holes is changed, which has an impact on the machining accuracy. The majority of pertinent studies concentrate on the rigid location approach for the entire blade, which results in a modest relative position error of the blade surface but still fails to give the exact position and axial direction of the film cooling holes of the deformed blade. In this paper, the entire deformation of the blade cross-section curve is divided into a number of deformation combinations of the mean line curve based on the construction method of the blade design intent. The exact location of the film cooling holes in the turbine blade with deviation is therefore efficiently solved by a flexible deformation of the blade that optimises the position and axial direction of the holes. The verification demonstrates that the novel method can significantly reduce both the contour deviation of the blade surface and the location issue of the film cooling holes. After machining experiments, the maximum position deviation of the holes is reduced by approximately 80% compared to the rigid location method of the entire blade, and the average value and standard deviation are also decreased by about 70%.

Keywords Turbine blade · Film cooling holes · Adaptive location · Blade deformation

1 Introduction

Aero-engines, gas turbines, and other blade machines depend heavily on their turbine blades, which are made of Ni-based single crystal superalloy and are cast to survive the harsh service environment of high temperature and high pressure. In order to obtain improved performance in terms of combustion efficiency and thrust-weight ratio, the turbine inlet temperature (1700–2000 K) has far exceeded the melting point (about 1700 K) of the turbine blade [1]. The film cooling method is normally suggested to enhance the high-temperature creep resistance and maintain the normal state of the turbine blade [2]. A coating of air film is created on the surface of the turbine blade by conducting cold air

through hundreds of tiny holes placed in the proper positions across the turbine blade. As a result, the blades are safeguarded by being separated from the hot gases.

The key to increasing the aero-engine's operational efficiency is to correctly machine the film cooling holes of the turbine blade [3], where two accuracy issues need to be resolved: exact dimension and accurate location. The film cooling holes have a deep depth and a relatively narrow radius, often between 0.2 and 0.8 mm, which are typical high-aspect-ratio micro holes, and are therefore challenging to produce using traditional techniques [4]. With the development of EDM and ultrashort pulse laser processing technology, as well as the maturity of related experiments, mathematical modelling, and other process methods [5, 6], the machining error of the micro hole gradually satisfies the accurate dimensional requirements of roundness, taper, contour, and other parameters. However, due to the intricate design and thin-walled structure, the cooling rate of the blade surface varies according to the curvature statues, which influences the casting process of the turbine blade and causes uneven deformation [7]. In other words, the real surface of the blade is not the same as the theoretical surface, and the theoretical position of the film cooling

✉ Jing Wang
wangjing@opt.ac.cn

¹ State Key Laboratory of Transient Optics and Photonics, Xi'an Institute of Optics and Precision Mechanics, Chinese Academy of Sciences, Xi'an 710119, China

² Key Laboratory of Vehicle Advanced Manufacturing, Measuring and Control Technology, Ministry of Education, Beijing Jiaotong University, Beijing 100044, China

hole is not necessarily on the real blade surface. The position deviation existed. Additionally, the creation of the air film and the direction of material removal depend greatly on the axial direction of the holes. As a result, during the actual machining process, the real surface normal should be considered [8]. The following outcomes may be attained if the film cooling holes are machined based on the theoretical position and axial direction: (1) The holes may not be perforated or the opposing wall may be damaged because of the discrepancy between the real depth and the theoretical depth; (2) the holes next to one other are crossed, which alters how cold air flows; (3) the interference with the holes may cause damage to the cavity ribs, compromising the structural integrity of the blade; (4) there is a chance that the machine tool and the blade will collide or interact, which could lead to production mishaps; and (5) The insulation and cooling effects will be impacted by the misalignment between the air film forming area and the blade surface.

To achieve this, researchers have optimised casting accuracy to the greatest extent possible by planning the parameters in advance with the law of the casting process on the effect of wall thickness and shrinkage of the turbine blade [9], or by analysing the deviation of the cast blade surface and compensating the casting moulds [10], or by performing finite element modelling of the casting process and predicting the casting results by numerical simulation [11]. Although these techniques have mostly succeeded in controlling the casting process and increasing the geometric accuracy of the blade surface, there are still some deviations, especially in the region of the turbine blade with a considerable curvature where tiny deviations are exponentially amplified.

Given the inevitable deviation, a methodical approach has been taken [12]: gathering the point cloud data of the real turbine blade using contact or non-contact measurements (sampling), utilising point cloud registration methods to determine the spatial relationship between the real blade and the theoretical blade (location), utilising reverse engineering to reconstruct the CAD model of the genuine blade (modelling), and finally, mapping the theoretical holes onto the real blade to calculate the real film cooling holes (distribution). Even though numerous high-precision measuring tools (such as CMMs, blue ray scanners) and algorithms are used to obtain accurate point clouds of the blade surface, and useful alignment techniques like principal component analysis (PCA), minimum potential energy (MPE), random sampling consistency (RANSAC), and iterative closest point (ICP) [13, 14] are used to achieve the precise position of the real blade, the transformation process is still rigid [15]. The local deviations still exist. As a result, the projected holes are unable to satisfy the real holes' design specifications in terms of both position and axial direction.

According to the previous discussion, the inverse modelling method can be proposed as modifying the surface shape of the theoretical blade to resemble as closely as possible the deformed surface of the real blade, and modifying the theoretical film cooling holes to achieve the precise location [16]. Reconstructing the geometric model of the blade is crucial. Currently, the inverse modelling of the blade is guided by the non-uniform rational B-spline (NURBS) fitting approach. By sweeping the cross-section curves and fitting the point cloud data, the blade surface is recreated [17, 18]. To increase the credibility of the point cloud, point cloud filtering techniques like homogeneous filter, statistical outlier removal, and chord-height deviation points are used. These techniques consider the errors, noise, and point deviations at large curvature positions introduced by the machining and subsequent measurements of the real blade [19]. However, the suggested inverse modelling method cannot result in a surface shape mapping between the theoretical blade and the actual blade. Fortunately, free-form deformation (FFD) technology, one of the widely used CAD model deformation techniques, can modify the control points of the created surface, changing the original CAD model in the process [20]. For instance, the use of rigid registration and FFD technology can ensure a perfect match in the blade body and a uniform allowance in the leading and trailing edge area when the precision-forged blade has a small deviation in the blade body area, but a large deviation in the leading and trailing edge area, or even torsional deformation in the blade [21]. This method can successfully finish the recovery and reconstruction of the CAD model of the blade while dealing with the issue of repairing deformed and damaged blades [22, 23]. Although the position matching issue between the real model and the theoretical model of the surface is solved by this method, it is challenging to manage the shape and precision of the leading and trailing edge regions.

This paper proposes an adaptive location method for film cooling holes based on blade design intent. Blade design intent means that the design process of the blade considers the influence of the mean line curve, thickness, and other design parameters of the cross-section curve on the geometric shape. Adaptive location indicates that for each manufactured blade, a personalised distribution of the film cooling holes is recalculated to satisfy the accuracy criteria. Therefore, based on the design principle of the blade cross-section curve, the position and normal direction of the points on the theoretical blade surface are transformed to achieve the precise location of the film cooling holes by the translation and rotation matrix calculated in the free deformation process from the theoretical cross-section curve to the real cross-section curve. The rest of the paper is structured as follows: The important parameters and the CAD modelling technique for the turbine blade are briefly introduced in Sect. 2. Section 3 provides a flexible deformation approach of the blade surface to determine the correspondence

between the theoretical blade and the actual blade. The related optimization procedure for the precise position of the holes is provided in Sect. 4. The position and machining of the holes in a turbine blade are discussed in Sect. 5, which serves as proof that the procedure described in this work is valid. In Sect. 6, the conclusions and prospect are covered.

2 Principles of parametric geometric modelling of blades

As a special free-form part, the main area of the blade consists of the leading edge, trailing edge, and convex and concave surfaces. After sweeping the 2D cross-section curves, the NURBS surfaces of the blade are constructed as shown in Fig. 1a. Obviously, the modelling accuracy can be improved by increasing the number of section curves. Therefore, creating precise section curves for the blade CAD model is the main challenge.

The mean line is established first in the blade design process in accordance with the demands of aerodynamic performance. Then, the various thicknesses are superimposed over the mean line to create the matching inscribed circles, and the envelope curve is the cross-section curve, as shown in Fig. 1b. The correlation of different regions of the cross-section curve is established based on the mean line curve, which realises the dimension reduction of the structure of the cross-section curve. In particular, the convex and concave curves are symmetrical with respect to the mean line curve, and the points in these curves are:

$$\begin{aligned} p_{cv} &= s + r \cdot n_{cv} \\ p_{cc} &= s + r \cdot n_{cc} \end{aligned} \tag{1}$$

where s is the discrete point of the mean line curve, p_{cv} and p_{cc} are the corresponding points of s in the convex and concave curves, respectively, the distance from these points to s is r referring to the radius of the inscribed circle, and n_{cv} and n_{cc} are the directions from these points to s , which are symmetrical with respect to the tangent t of s in the mean line. The leading and trailing edge curves are shown as circular

arcs at the endpoints of the mean line curve. Such section curves are designed in a forward manner.

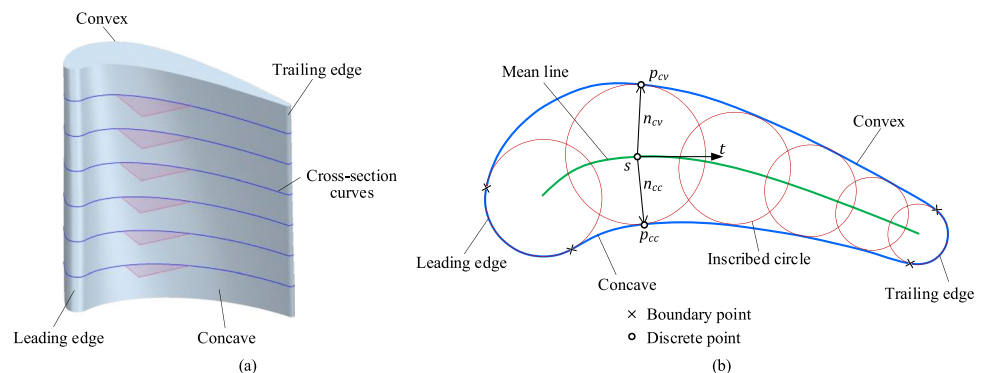
Considering that the theoretical model and measuring data of the blade contour are presented in the process of machining the film cooling holes, and it is difficult to directly obtain the mean line curve and thickness distribution of the corresponding cross-section curve, an inverse implement of the design method of the cross-section curve is applied to obtain the mean line curve and thickness distribution of the measured blade. Specifically, the algorithm is as follows: Figuring out the inscribed circles at various points along the section curve, then fitting the centres of each inscribed circles. The fitted curve is the mean line curve, and the diameter of the inscribed circle is assumed to be the thickness of the section curve. As a result, the parametric geometric modelling of the blade for the manufacturing process is achieved.

Next, the positions of the film cooling holes in the turbine blade are introduced, as shown in Fig. 2. In general, the holes are mainly distributed in groups in the path from root to tip of the blade and are located in the leading edge, concave, and convex surfaces. The adaptive method suggested in this research will be used to handle these surfaces because they underwent significant deformation throughout the casting process. The trailing edge surface will not be discussed for the non-existence of the film cooling holes.

3 Flexible deformation method of the blade surfaces

Due to the limits of the casting process, deviations in the turbine blades are unavoidable. However, these deviations may only be described as Euclidean distances between contours, which cannot account for the deformation between the theoretical and real blade surfaces. The geometric connection between the points and vectors of the concave and convex curves will be impacted by the deviations applied to deform the section curves directly because the concave and convex curves are symmetric with respect to the mean line curve. The parametric geometric modelling principle of the blade

Fig. 1 CAD models of **a** the turbine blade and **b** the cross-section curve



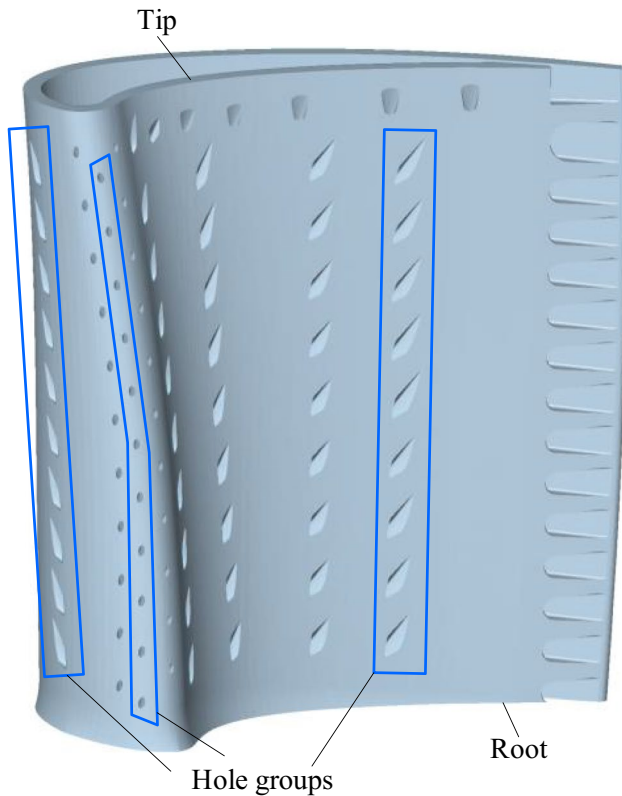


Fig. 2 The distribution of the film cooling holes

gives the way of superimposing the thickness on the mean line curve and reduces the dimension of the surface structure of the turbine blade. Therefore, it is essential to assess the deformation based on the mean line curve and transform the theoretical cross-section curve in order to match the real cross-section curve. This technique simultaneously increases the computational effectiveness of the algorithm and lowers the computational complexity of the concave and convex curves deformation.

3.1 Free form deformation method

Flexible deformation of the mean line curve using the FFD method is suggested to analyse deformation brought on by casting variations. The mean line curve properly satisfies the FFD method because it is a unidirectional, unclosed free curve. In contrast to FFD, which modifies the NURBS curve's control points, this article uses the real mean line curve as its target curve and transforms its discrete points to produce the new curve, as shown in Fig. 3. The distance between the corresponding points is defined as the translation, and the variation in the normal direction of the curve where the point is located is defined as the rotation, and the rotation angle is θ in the transformation process. s_{origin} and s_{target} are the discrete points of the original and target curves,

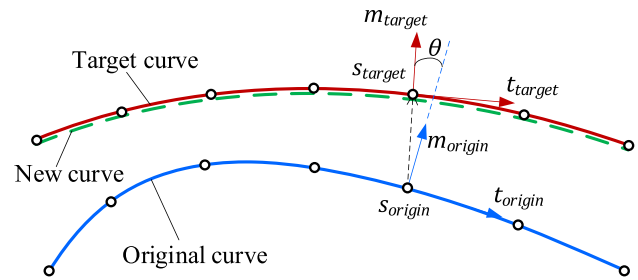


Fig. 3 Deformation of the free-form curve

respectively, and m and t are the normal and tangent directions of the discrete point, respectively.

The deformation matrix consisting of translations and rotations ensures that discrete points and vectors on the curve remain in the same relative geometric position to the curve as the curve is deformed. It should be noted that the cross-section curves and mean line curves treated in this paper are 2D shapes. Therefore, the translation matrix T_{warp} and rotation matrix R_{warp} using nonhomogeneous coordinates are represented as:

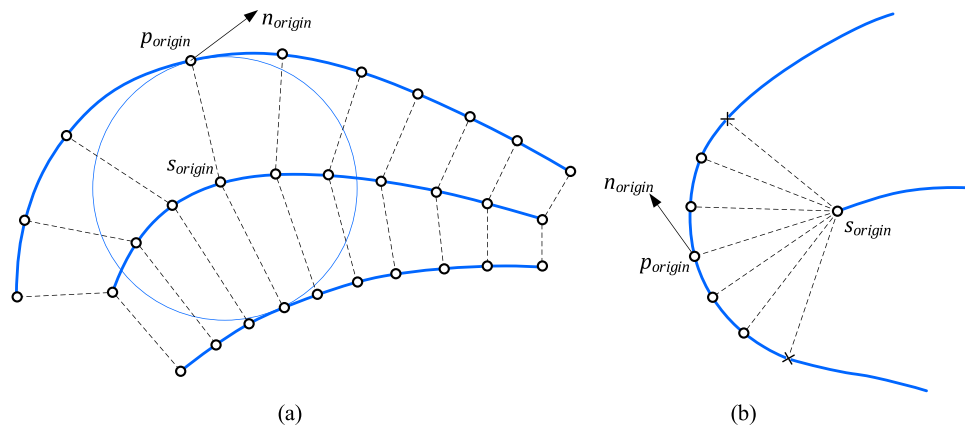
$$\begin{aligned} T_{\text{warp}} &= s_{\text{target}} - s_{\text{origin}} \\ R_{\text{warp}} &= \begin{bmatrix} \cos\theta & -\sin\theta \\ \sin\theta & \cos\theta \end{bmatrix} \end{aligned} \quad (2)$$

3.2 Deformation decomposition of the cross-section curve

With the FFD method for the mean line curve, the deformations implied by the manufacturing deviations in turbine blade can be decomposed. Prior to that, it is necessary to explain and define the discrete points that make up the section curves and mean line curve.

Considering that the concave and convex curves are symmetric with respect to the mean line curve, and the leading edge curve is related to the endpoint of the mean line curve, the mean line curve of the section curve is discretised according to the equal arc length method. The discrete points of the concave and convex curves are the points on those curves that are closest to the discrete points of the mean line curve (see Fig. 4a). The leading edge curve is discretized using the equal arc length approach based on the endpoint of the mean line curve, and the discrete points of the leading edge curve are generated (see Fig. 4b). Based on these explanations, the deformation process of the cross-section curve is illustrated using an arbitrary point on the theoretical mean line curve, where s_{origin} is the point in the theoretical mean line curve, p_{origin} is the corresponding point in the theoretical section curve (concave, convex or leading edge curves), and n_{origin} is the arbitrary vector of p_{origin} .

Fig. 4 The discrete points in **a** concave and convex curves and **b** leading edge curve



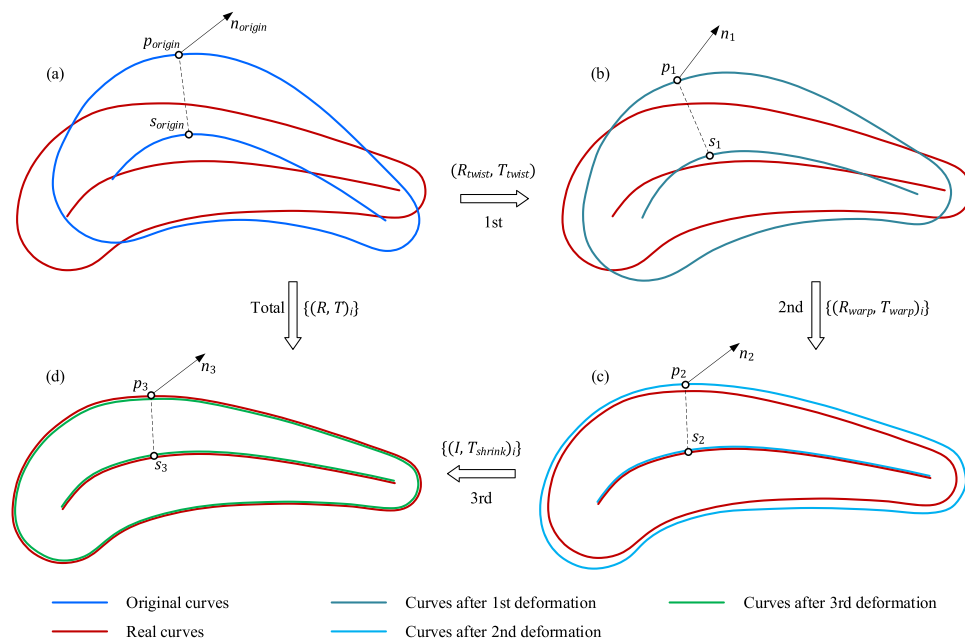
Based on the definition of the discrete points, the novel method of the deformation process of the cross-section curve is as follows: Under the initial condition of the rigid alignment of the theoretical and real blades, firstly, the theoretical and real mean line curves will be transformed to the position with the smallest average error (twisting deformation), and then the theoretical mean line curve will be deformed to the real mean line curve implementing the FFD method (warping deformation), and based on these operations, the thickness variation at the corresponding positions of the two curves will be calculated (shrinking deformation), so as to achieve the overall deformation of the theoretical cross-section curves. The s_{origin} , p_{origin} , and n_{origin} are deformed using the deformation order and the corresponding deformation matrix (see Fig. 5). In this case, the deformations of the discrete points of the concave and convex curves are calculated in the same process, and

a similar calculation process is proposed for the leading edge curve.

3.3 Twisting deformation process

After the initial rigid alignment between the theoretical and real blades, the twisting deformation describes the translation and rotation variations between the theoretical and real section curves when the relative deviations are minimal. Therefore, the 2D registration method, such as 2D ICP, is proposed to calculate the rotation matrix R_{twist} and translation matrix T_{twist} describing the twisting deformation. Additionally, the transformation of twisting deformation is rigid. Thus, the discrete points from the theoretical mean line, concave, convex, and leading edge curves have the same transformation matrices. The relative geometric values after twisting are represented as:

Fig. 5 Deformation process of the cross-section curves



$$\begin{aligned}
 s_1 &= R_{\text{twist}} \cdot s_{\text{origin}} + T_{\text{twist}} \\
 p_1 &= R_{\text{twist}} \cdot p_{\text{origin}} + T_{\text{twist}} \\
 n_1 &= R_{\text{twist}} \cdot n_{\text{origin}}
 \end{aligned}
 \tag{3}$$

where s_1 is the discrete point of the mean line curve after 1 deformation, p_1 is the discrete point of the section curves after 1 deformation, and n_1 is the vector of p_1 after 1 deformation. The twisting transformation is shown in Fig. 5a and b.

3.4 Warping deformation process

Following the twisting transformation, the warping deformation describes how the theoretical and real section curves differ in shape. The twisted mean line and section curves are warped using the FFD method, which is devised in this paper to calculate the translation and rotation of each discrete points. The calculation process of the translation matrix T_{warp} and the rotation matrix R_{warp} is shown in Sect. 3.1. In the deformation process of discrete points of the concave, convex, and mean line curves, the rotations are calculated through the matching normal direction of the mean line curve. When computing the deformations of the discrete points of the leading edge curve and the end point of the mean line curve, the rotations are determined by the vectors created by the discrete points of the leading edge curve and the endpoint of the mean line curve. Figure 6 illustrates the warping deformation processes from the region to be deformed to the target region at the concave, convex, and leading edge following the twisting process, respectively.

Therefore, the relative geometric values after warping are represented as:

$$\begin{aligned}
 s_2 &= s_1 + T_{\text{warp}} \\
 p_2 &= R_{\text{warp}} \cdot (p_1 - s_1) + T_{\text{warp}} + s_1 \\
 n_2 &= R_{\text{warp}} \cdot n_1
 \end{aligned}
 \tag{4}$$

where s_2 is the discrete point of the mean line curve after 2 deformations, p_2 is the discrete point of the section curves

after 2 deformations, and n_2 is the vector of p_2 after 2 deformations. The warping transformation is shown in Fig. 5b and c.

It should be emphasised that each discrete point on the mean line curve experiences a distinct deformation matrix during warping deformation, which must be calculated independently.

3.5 Shrinking deformation process

Since the warping deformation has corrected the deviation of the two mean line curves, the shape of the section curve after warping is similar to the real section curve. The only discrete points of the cross-section curves that still have a deviation are caused by the shrinking deformation. Figure 7 illustrates the concave, convex, and leading edge shrinking deformation processes from the to-be-deformed zone to the target region following the warping process. The rotation is no longer included, and the translation matrix T_{shrink} is represented as

$$T_{\text{shrink}} = p_{\text{target}} - p_2
 \tag{5}$$

Therefore, the relative geometric values after shrinking are represented as

$$\begin{aligned}
 s_3 &= s_2 \\
 p_3 &= p_2 + T_{\text{shrink}} \\
 n_3 &= n_2
 \end{aligned}
 \tag{6}$$

where s_3 is the discrete point of the mean line curve after 3 deformations, p_3 is the discrete point of the section curves after 3 deformations, and n_3 is the vector of p_3 after 3 deformations. The warping transformation is shown in Fig. 5c–d.

Similarly, during shrinking deformation, each discrete point on the mean line curve has a specific deformation matrix that must be calculated separately.

Fig. 6 The warping deformation process of the **a** concave, convex, and **b** leading edge regions

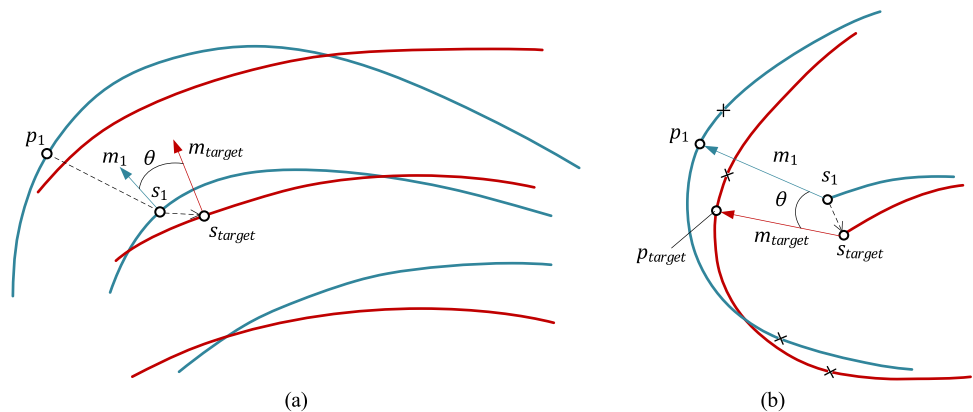
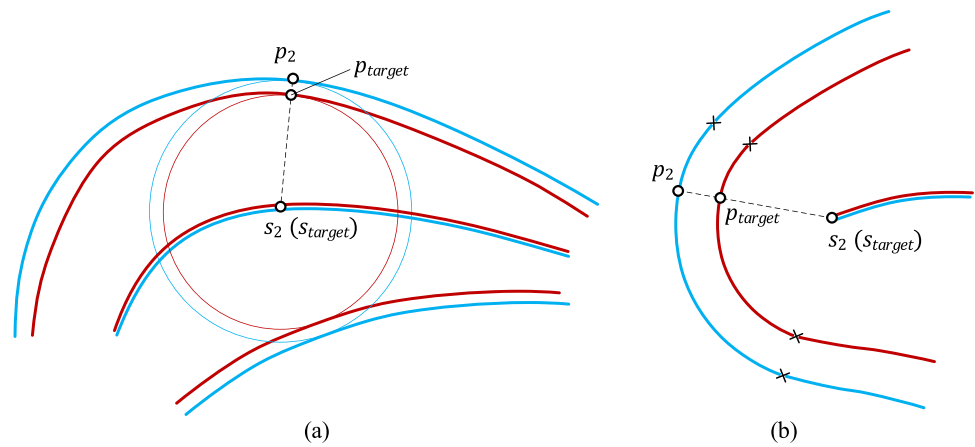


Fig. 7 The shrinking deformation process of the **a** concave, convex, and **b** leading edge regions



3.6 Deformation of whole blade surfaces

Combining the above twisting, warping, and shrinking deformations, the discrete point p_{origin} and vector n_{origin} on the theoretical cross-section curve are finally transformed into the following form:

$$p_3 = R_{warp} \cdot R_{twist} \cdot p_{origin} - R_{warp} \cdot R_{twist} \cdot s_{origin} + R_{twist} \cdot s_{origin} + T_{twist} + T_{warp} + T_{shrink} \tag{7}$$

$$n_3 = R_{warp} \cdot R_{twist} \cdot n_{origin}$$

As a result, the translation matrix T and rotation matrix R of the flexible deformation process of the theoretical cross-section curve to the real cross-section curve are represented as:

$$T = -R_{warp} \cdot R_{twist} \cdot s_{origin} + R_{twist} \cdot s_{origin} + T_{twist} + T_{warp} + T_{shrink}$$

$$R = R_{warp} \cdot R_{twist} \tag{8}$$

where the deformation process is shown in Fig. 5a–d.

Applying this method, the deformation field of the cross-section curve is created by calculating the flexible deformation matrix for each discrete point corresponding to the mean line curve on the concave, convex, and leading edge curves. Finally, the method is extended to all the cross-section curves to complete the spatial transformation of the discrete points of the theoretical blade surface, which constitutes the CAD model of the deformed blade surface and realises the flexible deformation of the whole blade surfaces.

4 Precision location and optimization of holes

4.1 Analysis of deformed holes

Based on the overall flexible deformation data of the blade,

the position and axial direction of the theoretical film cooling holes are transformed to determine the position and axial direction of the holes on the real blade surface. The fitting method of the surface parameter domains is used to calculate the deformation of the theoretical holes because the theoretical positions of the film cooling holes are not exactly the same as the discrete points when the transformation matrix of the theoretical blade is calculated.

For blade CAD models, the concave, convex, and leading edge surfaces are generally composed of NURBS surfaces, which are represented with a parameter u within the section curves and a parameter v between the curves. Meanwhile, the deformation, including translation matrix T and rotation matrix R , can be represented as three values x , y , and θ . Combining the above variables, three fitting functions $x = f_1(u, v)$, $y = f_2(u, v)$, and $\theta = f_3(u, v)$ are constructed based on the parameters (u, v) of the discrete points of the deformed blade surfaces and the deformations (x, y, θ) .

After calculating the (u, v) parameters of the theoretical holes on the corresponding surfaces and solving these three fitting functions, the deformation of the corresponding holes can be determined, and the associated deformation matrices can be built. Since the points on the blade surface are 3D data and the deformations are 2D data, the translation matrix T_{hole} and the rotation matrix R_{hole} of the real holes are represented as:

$$\begin{aligned} T_{\text{hole}} &= [x, y, 0]^T \\ R_{\text{hole}} &= \begin{bmatrix} \cos\theta & -\sin\theta & 0 \\ \sin\theta & \cos\theta & 0 \\ 0 & 0 & 1 \end{bmatrix} \end{aligned} \quad (9)$$

Therefore, the relative information of the deformed holes can be obtained as follows:

$$\begin{aligned} p_{\text{hole,def}} &= R_{\text{hole}} \cdot p_{\text{hole,origin}} + T_{\text{hole}} \\ n_{\text{hole,def}} &= R_{\text{hole}} \cdot n_{\text{hole,origin}} \end{aligned} \quad (10)$$

where $p_{\text{hole,origin}}$ and $n_{\text{hole,origin}}$ are the position and axial direction of the film cooling holes in the theoretical blade, respectively, and $p_{\text{hole,def}}$ and $n_{\text{hole,def}}$ are the position and axial direction of the film cooling holes in the flexible deformed blade, respectively.

4.2 Optimization and adjustment of holes

There are still small deviations between the positions of the deformed holes and the real blade surfaces, and these deviations may be caused by the non-smoothness of the local surface. Therefore, it is necessary to optimise the position and axial direction of the flexible deformed holes based on the design principle of the film cooling holes.

When designing the film cooling holes, the path from the root to the tip of the blade is typically considered the basic direction, and the holes in this direction will be considered to be the basic group. The direction of the arc length parameter of the cross-section curve will guide the planning of

various groups (see Fig. 2). The holes in the same groups have essentially the same sizes, axial directions, and places along the same sweeping curve (see Fig. 8a). However, the axial directions of the holes within the group may not be similar in the leading edge surface of the blade. Therefore, it is necessary to divide subgroups based on the similarity of theoretical axes. The hole axes within the subgroups are essentially consistent (see Fig. 8b). Additionally, the subgroup is considered the fundamental group in the optimisation process.

Therefore, an optimisation method is developed:

Step 1: A low-order virtual curve is fitted for the flexible deformed holes $\{p_i\}$ in the group. The appropriate projection curve is created after projecting the virtual curve onto the real blade surface. The ultimate, exact locations of the real holes are the corresponding holes on the projection curve.

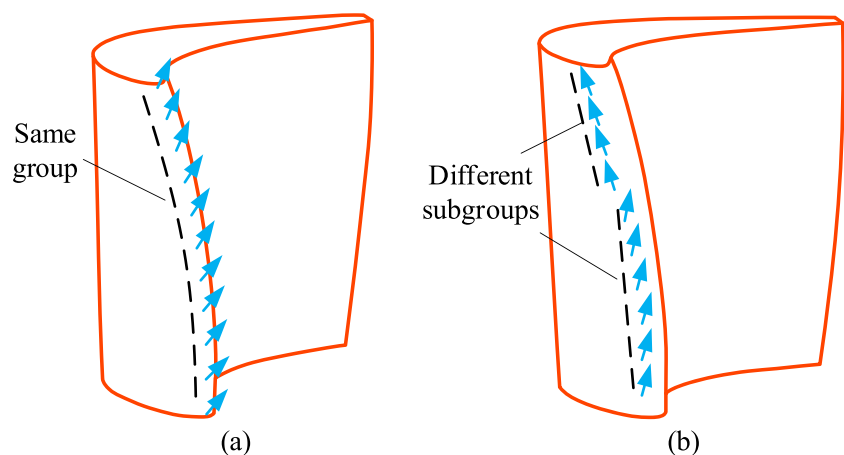
Step 2: The Quaternionic interpolation of the axial direction $\{n_i\}$ of the flexible deformed holes in the direction of the arc length parameter of the projection curve is implemented based on the projected positions of the holes. It should be noticed that the axes in the subgroups are proposed to be optimised when existing the subgroups.

Following the aforementioned optimization, the precise position and axial direction of the film cooling holes are obtained, and the adaptive location of the film cooling holes is achieved.

5 Case and discussion

In order to verify the accuracy of the adaptive location method of the film cooling holes proposed in this paper, the following experiment processes are adopted. Firstly, the SHINING 3D OptimScan 5 M Plus-200 is applied to measure the casting turbine blade and create a point cloud

Fig. 8 The similar axial directions **a** in the same group and **b** in different subgroups



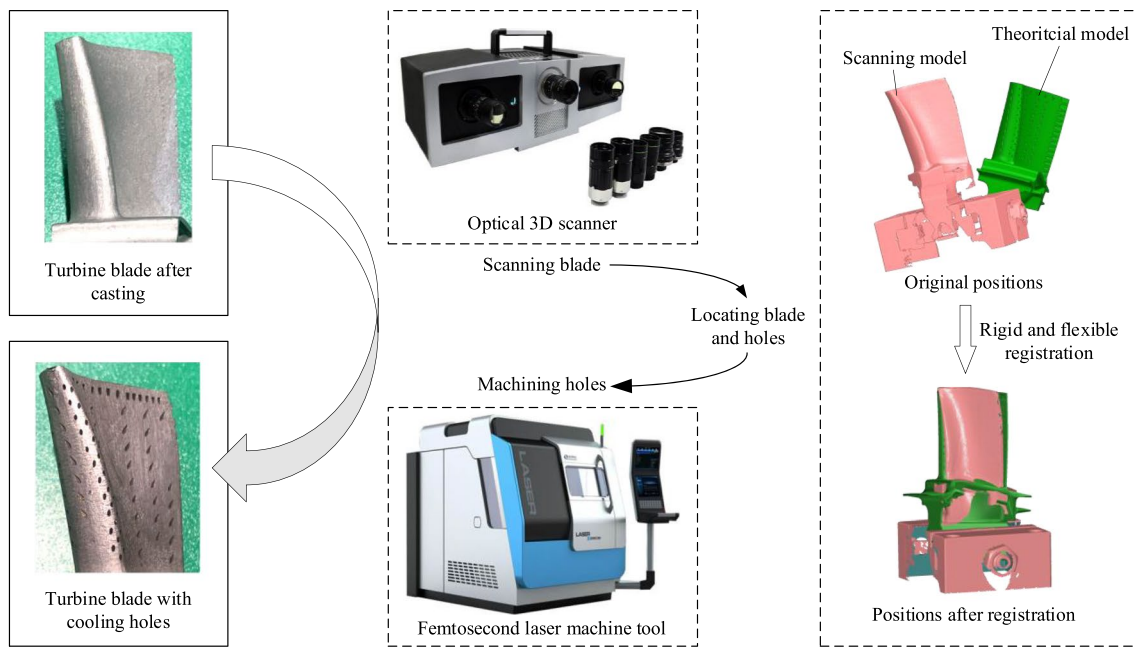


Fig. 9 Adaptive location and machining framework for film cooling holes

of the blade surfaces. This measuring equipment is a high-precision 3D inspection scanner with narrow-band blue light source. The single-shot accuracy is 0.01 mm. The preliminary alignment and position are then achieved by using six points provided by the turbine blade design department as the matching points of ICP algorithm to transform the measured point cloud data with the theoretical blade. Based on this, the adaptive method developed in this paper is used to predict the position and axial direction of the real holes. Finally, the five-axis femtosecond laser processing equipment created by the Xi'an Institute of Optics and Precision Mechanics is then used to process the calculated holes. Figure 9 depicts the entire procedure along with the hardware and software.

The blade is approximately $35 \times 25 \times 8$ mm in size, and because it is clamped to a fixture, there are more than 3 million points and more than 6 million triangular meshes of the blade and fixture after 3D scanning. The calculation time of the flexible deformation process of the blade is mainly related to the number of the blade sections, and the algorithms are programmed through the secondary development of Siemens NX 1899. The computation time for a single cross-section is less than 5 min on a PC with an Intel(R) Core(TM) i7-11800H CPU (RWI 4.8 GHz), a 16 GB RAM, an NVIDIA GeForce RTX 3060 Laptop GPU, and a 512 GB SSD. The sampling and fitting of the cross-section curves of the point cloud take about 4 min. The adaptive approach presented in this paper has a running time that is less than a minute. The whole computation time is under 22 min when the deformed blade is rebuilt using 4 cross-sections.

It should be noted that the original coordinate system of the scanned point cloud of the turbine blade is related to the spatial position and state of the 3D scanner; it is difficult to predict the coordinate system of the measured point cloud in advance. The six-point ICP algorithm is used to produce the initial transformation, which is an essential first step. However, when the spatial position of the measured point cloud and the theoretical blade differs significantly from each other and the application of the six-point ICP algorithm is unable to obtain an accurate location, other coarse alignment methods, such as principal component analysis, minimum potential energy, random sampling consensus, and other algorithms, can be considered first. Then, the six points provided by the design department are carried out for subsequent operations.

Different location results are examined in the experiment and contrasted, including (I) the three-plane location method based on fixture, (II) the ICP method of blade surfaces, (III) the ICP method of six points from the design department, and (IV) the adaptive location method in this paper, as shown in Fig. 10. The regions for location calculation are highlighted as yellow. Based on these location methods, the deviations of the real blade and the theoretical blade as well as the distribution of the film cooling holes are compared to verify the accuracy of the adaptive location method of the film cooling holes proposed in this paper.

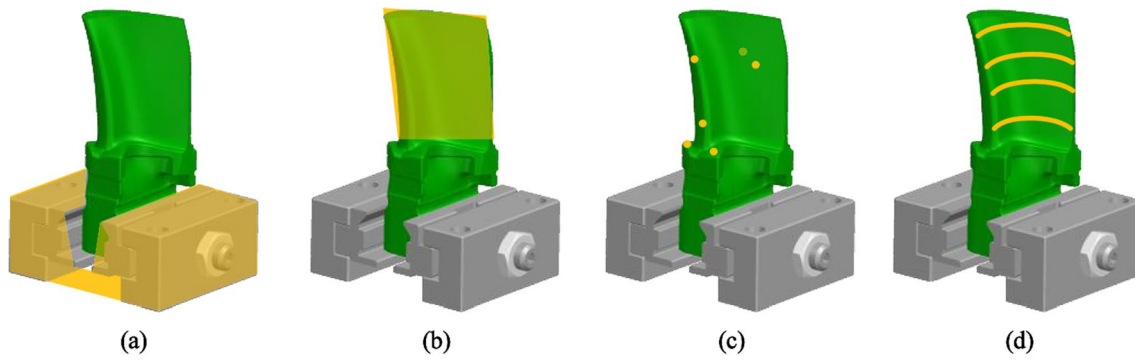


Fig. 10 Regions for location calculation of **a** I, **b** II, **c** III, and **d** IV methods

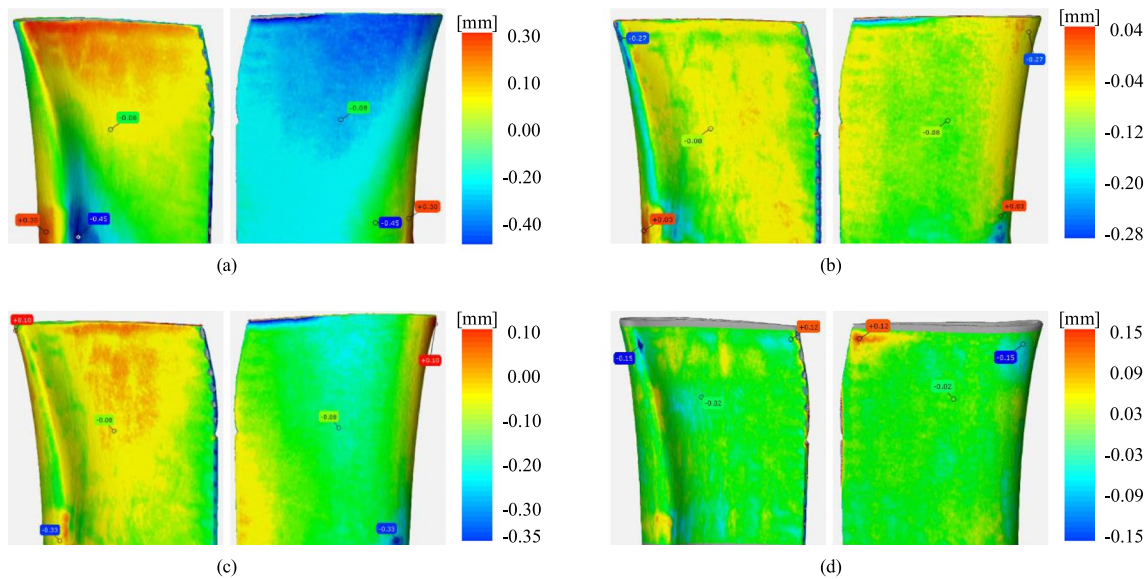


Fig. 11 Deviation cloud maps of **a** I, **b** II, **c** III, and **d** IV methods

Table 1 Deviation statistics of cloud map (mm)

Location methods	Maximum	Minimum	Average	Standard deviation
I	0.297	-0.450	-0.084	0.194
II	0.027	-0.275	-0.083	0.043
III	0.095	-0.329	-0.080	0.069
IV	0.124	-0.149	-0.020	0.025

5.1 Deviations of blade surfaces

The related deviation cloud maps can be created for the four location methods mentioned above as shown in Fig. 11. The first three cloud maps among them describe the deviation of the real blade calculated by the corresponding location methods from the theoretical blade, while the last cloud map describes the deviation of the real blade calculated by

Method III from the theoretical blade calculated by Method IV. The deviation statistics are shown in Table 1.

According to the aforementioned deviation statistics, Method I yields the worst location outcomes in terms of maximum, minimum, average, and standard deviation. The explanation for this is because even if the fixture is perfectly aligned when the blade is manually clamped, the ultimate position of the blade may not be exact due to differing clamping strengths. At the same time, the lack of clamping accuracy amplifies the location mistakes of the blade surfaces. While Methods II and III both employ the ICP algorithm and select distinct model regions, their end results are similar. Method II outperforms Method III somewhat. The maximum and minimum deviations, as well as the standard deviation, of Methods II and III, have all decreased when compared to Method I. Because the distances between the real model located by Methods I–III and the theoretical model are quite close, the positive and negative deviations

cancel each other out when computing the average value, leaving Methods I–III with almost the same average values. The Method IV suggested in this paper conducts overall flexible deformation on the blade surfaces and has a reduced average value and a more uniform distribution of deviations. In comparison to other approaches, the average value falls by almost 75%. The standard deviation falls by 41.9% in comparison to Method II, which has the strongest location effect. Therefore, the overall flexible deformation of surfaces in this paper is demonstrated to be effective.

5.2 Distribution of film cooling holes

The theoretical blade is suggested as the reference during the comparison procedure for blade surface deviation. However, the deformed turbine blade during the hole measuring process causes the datum of film cooling holes to shift. Based just on the theoretical position, it is challenging to evaluate the quality of the actual holes. Therefore, it is necessary to detect the geometric information of the holes based on the real location of the film cooling holes in the real turbine blade. It is suggested to use optical detection, CT, and other testing tools. However, there is currently no quantitative method to determine whether real holes still fulfil design specifications even after their reference is lost. As a result, the femtosecond laser is used to machine the real holes predicted by Method IV, and the position and radius are then determined. The real holes are compared with the holes predicted by Methods I–IV. The theoretical holes are projected onto the real blade surfaces to produce the predicted holes from Methods I to III. The deviations of the hole positions are shown in Fig. 12. The horizontal coordinate is the hole number and the vertical coordinate is the hole deviation. The deviation statistics are shown in Table 2. Only those in groups 1 (in the convex surface), 5 (in the leading edge surface), and 9 (in the concave surface) were chosen for comparison because of the sheer volume of film cooling holes that were present.

The deviation data for film cooling holes shows that the holes computed using Method I have a larger deviation, and

Table 2 Deviation statistics of hole position (mm)

Location methods	Maximum	Minimum	Average	Standard deviation
I	0.242	0.005	0.099	0.062
II	0.150	0.002	0.061	0.043
III	0.162	0.004	0.056	0.040
IV	0.033	0.003	0.019	0.009

the tendency is consistent with the surfaces. The findings of Method IV were noticeably superior to those of Methods II and III for group 1 in the convex surface and group 5 in the leading edge surface. The deviations in group 9 of Methods II–IV were superior to one another because group 9 had a reduced surface deformation. The greatest deviation of the hole position for Method IV, however, fell by nearly 80% when viewed holistically, and the average and standard deviation also decreased by about 70% when compared to Methods I–III. In addition, the minimal deviations for the four approaches have a low absolute value. The effectiveness of Method IV established in this paper for the precise location for the film cooling holes of the turbine blade is demonstrated by all of these comparison results.

In addition to the location and optimization of the holes, the axial direction of the film cooling holes is optimised by Method IV in this paper. The angle between the axial direction of the holes and the normal direction of the blade surface, which was computed by several ways, was examined to demonstrate the correctness of the localization and optimization method. Considering that among Methods I–III, Methods II and III have the smallest deviation in the hole position, and the difference is not significant, Method III is chosen for comparison with Method IV. In Method III, the real holes are created by projecting the theoretical holes to the real surface. The hole axes are not changed throughout the locating process. Therefore, the real axial direction of the film cooling hole is the theoretical axial direction. Based on the aforementioned calculations, the angle between the axial direction of the theoretical hole and the normal

Fig. 12 The position deviations of holes located by different methods

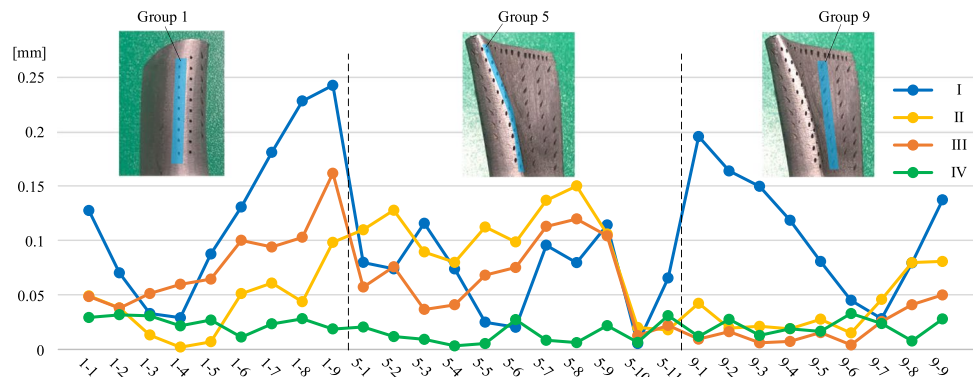


Fig. 13 The angles between axial and normal directions of the theoretical and real blades located by Methods III and IV

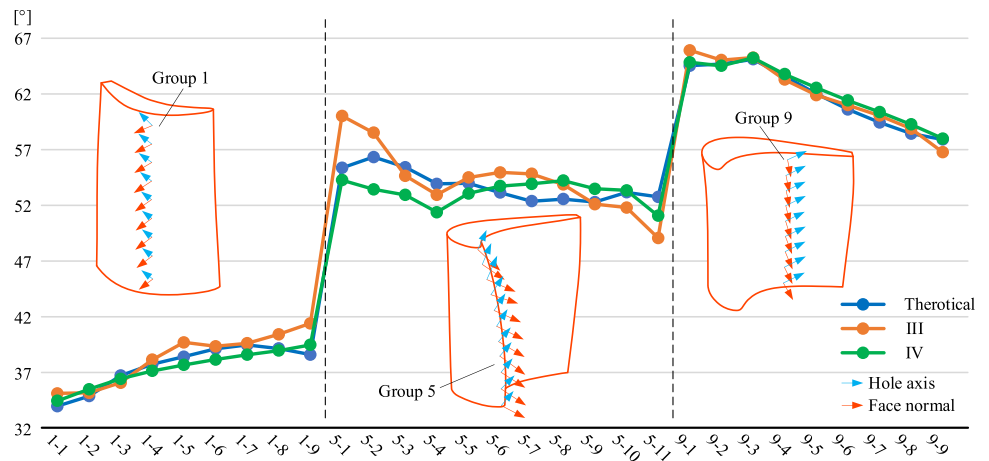


Fig. 14 The angle deviations caused by Methods III and IV

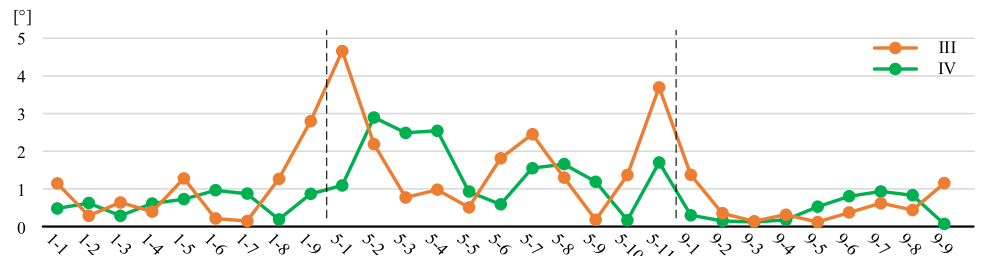


Table 3 Deviation statistics of the angle between axial and normal directions (°)

Location methods	Maximum	Minimum	Average	Standard deviation
III	4.659	0.124	1.140	1.111
IV	2.896	0.073	0.911	0.749

direction of the theoretical blade and the angle between the axial direction of the real hole and the normal direction of the real blade calculated by Methods III and IV are obtained, as shown in Fig. 13. The horizontal coordinate is the hole number and the vertical coordinate is the angle between the axial direction and the normal direction.

Based on the angle between the axial direction and the normal direction of the theoretical blade, the angle deviations of the real blade located by the Methods III and IV are obtained, as shown in Fig. 14. The horizontal coordinate is the hole number and the vertical coordinate is the angle deviations. Since the positive change of the angle direction cannot be determined, the absolute values are utilised for all the angle deviations, as shown in Table 3.

It can be shown that while the angle deviation under the various methods varies little in the concave and convex surfaces, it drastically changes in the leading edge surfaces with large curvatures under Methods III and IV. However,

as can also be inferred from the data in Table 3, the overall change of the angle computed by Method IV is relatively steady. Additionally, the angle variation of Method IV is noticeably better than that of Method III at the tip or root regions, such as Points 1–1, 1–9, 5–1, 5–11, 9–1, and 9–9, which further demonstrates the efficacy of the current method in this paper for the precise axial location of the film cooling holes of the deformed turbine blade.

The following conclusions can be reached from the experimental data and statistical analysis:

1. Compared with the ICP method of the blade surfaces (i.e., Method II), the overall flexible deformation of the theoretical model using the method in this paper produced a more homogeneous distribution of deviations of the surfaces, with a decrease of about 75% in the mean value and 41.9% in the standard deviation.
2. When compared with the real film cooling holes after adopting the ICP method of the blade surfaces (i.e., Method II) or the ICP method of six points (i.e., Method III), the maximum deviation of the position of the film cooling holes after adopting the method in this paper has decreased by about 80%, and the mean value and standard deviation have also decreased by about 70%. Also, the angle between the axial direction of the film cooling holes and the normal direction of the blade surface is

more consistent with the distribution of the angle on the theoretical blade.

6 Conclusions

An adaptive location method for the film cooling holes is provided based on the design intent of the blade in order to address the impact of the casting deviation of the turbine blade on the location datum of the holes. The free transformation matrix from the theoretical cross-section curve to the real cross-section curve is constructed to deform the blade surfaces flexibly, and the accurate location of the position and axial direction of the film cooling holes is satisfied. This is done by decomposing the casting deviations of the cross-section curves into the twisting, warping, and shrinking deformations based on the theoretical mean line curve. The main conclusions are the following:

1. The implementation of the overall flexible deformation method of the blade significantly improves location accuracy of the blade surface when compared to the rigid transformation method (ICP) of the overall blade surfaces, with an average error reduction of about 75% and a standard deviation reduction of 41.9%. The technique can be applied to the adaptive machining of various deformed blade surfaces in addition to the deformation and reconstruction of the casting turbine blade.
2. When compared to the position of the film cooling holes after using the rigidity transformation method (ICP) of the overall blade surfaces, the maximum deviation of the position of the film cooling holes by applying the method of this paper is reduced by about 80%, and the mean and standard deviation are also reduced by about 70%. The distribution of the angle between the axial direction and the normal direction is more consistent with the angle on the theoretical blade. So the improvement of the location accuracy of the film cooling holes is significant, and the final deviation meets the machining requirements.

Finally, there are still a few issues. In addition to changing the blade surface, the casting process also causes variations in the turbine blade's internal cavity. These deviations influence how the film cooling holes inside the blade interact with one another and vary the depths of the holes, both of which require more study.

Author contribution All authors contributed to the study conception and design. Investigation, methodology, software, material preparation, data collection, visualisation, and analysis were performed by Yaohua Hou, Jing Wang, and Jiawei Mei. Resources, supervision and project administration were performed by Jing Wang and Hualong Zhao. The

first draft of the manuscript was written by Yaohua Hou and all authors commented on previous versions of the manuscript. All authors read and approved the final manuscript.

Funding This work was supported by Natural Science Basic Research Plan in Shaanxi Province of China (no. 2022JQ-473), Young Talent Fund of Xi'an Association for Science and Technology (no. 095920221309), and National Natural Science Foundation of China (no. 52205438).

Declarations

Competing interests The authors declare no competing interests.

References

1. Zhang J, Zhang S, Wang C, Tan X (2020) Recent advances in film cooling enhancement: a review. *Chin J Aeronaut* 33:1119–1136. <https://doi.org/10.1016/j.cja.2019.12.023>
2. Chen P, Shi W, Li X, Ren J, Jiang H (2021) Numerical study of using dean vortices to enhance the film cooling performance for fan shaped hole. *Int J Therm Sci* 165:106913. <https://doi.org/10.1016/j.ijthermalsci.2021.106913>
3. Montomoli F, Massini M, Salvadori S, Martelli F (2011) Geometrical uncertainty and film cooling: fillet radii. *J Turbomach* 134:1–8. <https://doi.org/10.1115/1.4003287>
4. Cheng YQ, Li WL, Jiang C, Wang G, Xu W, Peng QY (2022) A novel cooling hole inspection method for turbine blade using 3D reconstruction of stereo vision. *Meas Sci Technol* 33:. <https://doi.org/10.1088/1361-6501/ac39d0>
5. Li ZY, Wei XT, Guo YB, Sealy MP (2015) State-of-art, challenges, and outlook on manufacturing of cooling holes for turbine blades. *Mach Sci Technol* 19:361–399. <https://doi.org/10.1080/10910344.2015.1051543>
6. Zhao W, Yu Z (2018) Self-cleaning effect in high quality percussion ablating of cooling hole by picosecond ultra-short pulse laser. *Opt Lasers Eng* 105:125–131. <https://doi.org/10.1016/j.optlaseng.2018.01.011>
7. Dong YW, Li XL, Zhao Q, Yang J, Dao M (2017) Modeling of shrinkage during investment casting of thin-walled hollow turbine blades. *J Mater Process Technol* 244:190–203. <https://doi.org/10.1016/j.jmatprotec.2017.01.005>
8. Li L, Li B, Zhang R, Xue Z, Wei X, Chen L (2023) Geometric parameters measurement for the cooling holes of turbine blade based on microscopic image sequence topographical reconstruction. *Meas J Int Meas Confed* 210:112562. <https://doi.org/10.1016/j.measurement.2023.112562>
9. Tian G, Bu K, Zhao D, Zhang Y, Qiu F, Zhang X, Ren S (2018) A shrinkage prediction method of investment casting based on geometric parameters. *Int J Adv Manuf Technol* 1035–1044. <https://doi.org/10.1007/s00170-018-1618-5>
10. Ren S, Bu K, Mou S, Zhang R, Bai B (2023) Control of dimensional accuracy of hollow turbine blades during investment casting. *J Manuf Process* 99:548–562. <https://doi.org/10.1016/j.jmapro.2023.05.077>
11. Yang L, Chai LH, Liang YF, Zhang YW, Bao CL, Liu SB, Lin JP (2015) Numerical simulation and experimental verification of gravity and centrifugal investment casting low pressure turbine blades for high Nb-TiAl alloy. *Intermetallics* 66:149–155. <https://doi.org/10.1016/j.intermet.2015.07.006>
12. Xue-Cheng Xi, Jian W, Si-Meng Z, Jie-Yu Ma, Wang-Sheng Z (2023) Adaptive drilling of film cooling holes of turbine vanes

- based on registration of point clouds. *IEEE Trans Industr Inf*. <https://doi.org/10.1109/TII.2023.3254664>
13. Cheng X, Li Z, Zhong K, Shi Y (2017) An automatic and robust point cloud registration framework based on view-invariant local feature descriptors and transformation consistency verification. *Opt Lasers Eng* 98:1339–1351. <https://doi.org/10.1016/j.optlaeng.2017.05.011>
 14. Wu Z, Wang Y, Mo Y, Zhu Q, Xie H, Wu H, Feng M, Mian A (2022) Multiview point cloud registration based on minimum potential energy for free-form. *IEEE Trans Instrum Meas* 71:1–14. <https://doi.org/10.1109/TIM.2022.3169559>
 15. He W, Li Z, Guo Y, Cheng X, Zhong K, Shi Y (2018) A robust and accurate automated registration method for turbine blade precision metrology. *Int J Adv Manuf Technol* 97:3711–3721. <https://doi.org/10.1007/s00170-018-2173-9>
 16. Mahboubkhah M, Aliakbari M, Burvill C (2016) An investigation on measurement accuracy of digitizing methods in turbine blade reverse engineering. *J Eng Manuf Part B*. <https://doi.org/10.1177/0954405416673681>
 17. Hou Y, Zhang D, Mei J, Zhang Y, Luo M (2019) Geometric modelling of thin-walled blade based on compensation method of machining error and design intent. *J Manuf Process* 44:327–336. <https://doi.org/10.1016/j.jmapro.2019.06.012>
 18. Wilson JM, Piya C, Shin YC, Zhao F, Ramani K (2014) Remanufacturing of turbine blades by laser direct deposition with its energy and environmental impact analysis. *J Clean Prod* 80:170–178. <https://doi.org/10.1016/j.jclepro.2014.05.084>
 19. Yang F, Cai Z, Chen Y, Dong S, Deng C, Niu S, Zeng W, Wen S (2022) A robotic polishing trajectory planning method combining reverse engineering and finite element mesh technology for aero-engine turbine blade TBCs. *J Therm Spray Technol* 31:2050–2067. <https://doi.org/10.1007/s11666-022-01434-9>
 20. Li Y, Ni J (2009) Constraints based nonrigid registration for 2D blade profile reconstruction in reverse engineering. *J Comput Inf Sci Eng* 9:1–9. <https://doi.org/10.1115/1.3184602>
 21. Zhang Y, Chen ZT, Ning T (2015) Reverse modeling strategy of aero-engine blade based on design intent. *Int J Adv Manuf Technol* 81:1781–1796. <https://doi.org/10.1007/s00170-015-7232-x>
 22. Rong Y, Xu J, Sun Y (2014) A surface reconstruction strategy based on deformable template for repairing damaged turbine blades. *Proc Inst Mech Eng Part G J Aeronaut Eng* 228:2358–2370. <https://doi.org/10.1177/0954410013517091>
 23. Li L, Li C, Tang Y, Du Y (2017) An integrated approach of reverse engineering aided remanufacturing process for worn components. *Robot Comput Integr Manuf* 48:39–50. <https://doi.org/10.1016/j.rcim.2017.02.004>

Publisher's Note Springer Nature remains neutral with regard to jurisdictional claims in published maps and institutional affiliations.

Springer Nature or its licensor (e.g. a society or other partner) holds exclusive rights to this article under a publishing agreement with the author(s) or other rightsholder(s); author self-archiving of the accepted manuscript version of this article is solely governed by the terms of such publishing agreement and applicable law.